Asymmetric nuclear matter from an extended Brueckner-Hartree-Fock approach

W. Zuo,[1,*] I. Bombaci,[2,3] and U. Lombardo[1,4]
[1]*INFN-LNS, 44 Via S. Sofia, I-95123 Catania, Italy*
[2]*Dipartimento di Fisica, Università di Pisa, via Buonarroti, 2, I-56127 Pisa, Italy*
[3]*I.N.F.N., Sezione di Pisa, via Buonarroti, 2, I-56127 Pisa, Italy*
[4]*Dipartimento di Fisica, 57 Corso Italia, I-95129 Catania, Italy*
(Received 30 November 1998; published 6 July 1999)

The properties of isospin-asymmetric nuclear matter have been investigated in the framework of the extended Brueckner-Hartree-Fock approximation at zero temperature. Self-consistent calculations using the Argonne V_{14} interaction are reported for several values of the asymmetry parameter $\beta=(N-Z)/A$, ranging from symmetric nuclear matter to pure neutron matter. The binding energy per nucleon fulfills the β^2 law in the whole asymmetry range. The symmetry energy is calculated for different densities and discussed in comparison with other predictions. At the saturation point it is in fairly good agreement with the empirical value. The present approximation, based on the Landau definition of quasiparticle energy, is investigated in terms of the Hugenholtz–Van Hove theorem, which is proved to be fulfilled with a good accuracy at various asymmetries. The isospin dependence of the single-particle properties is discussed, including mean field, effective mass, and mean free path of neutrons and protons. The isospin effects in nuclear physics and nuclear astrophysics are briefly discussed. [S0556-2813(99)03108-8]

PACS number(s): 25.70.−z, 13.75.Cs, 21.65.+f, 24.10.Cn

I. INTRODUCTION

Within the general interest for the equation of state (EOS) of nuclear matter in nuclear physics as well as in nuclear astrophysics, increasing attention is currently paid to the isospin degree of freedom.

The EOS of isospin asymmetric nuclear matter plays a central role for our understanding of astrophysical phenomena like supernova explosions, neutron stars structure, x-ray bursts, neutron stars merging, and possibly γ-ray bursts. The study of asymmetric nuclear matter represents also the first step for a microscopic theory of the structure of nuclei far from the valley of beta stability. This ''terra incognita'' is going to be explored in the near future thanks to a new generation of experimental facilities with high intensity radioactive ion beams. Moreover, dynamical simulations of collisions between neutron-rich nuclei show that the main reaction mechanisms including fragmentation are quite sensitive to the density dependence of the nuclear symmetry energy [1,2]. Such calculations mainly make use of phenomenological Skyrme-like forces where the symmetry energy at high density can also be in strong disagreement with the one extracted from the microscopic predictions.

On a microscopic basis the EOS of asymmetric nuclear matter has been studied within the variational approach [3–5] as well as relativistic [6–11] and nonrelativistic [12] Brueckner-Bethe-Goldstone (BBG) theory. Within the Brueckner-Hartree-Fock (BHF) approximation to the BBG theory a systematic study of isospin effects on the EOS of asymmetric nuclear matter has been carried out in Ref. [12], where a separable version [13] of the Paris potential [14] was adopted to describe the two-body nuclear force.

Beside the bulk properties (EOS), the authors of Ref. [12] focused also on the single-particle (s.p.) properties of neutrons and protons in isospin-asymmetric nuclear medium. The neutron and proton s.p. potentials were calculated [12] to the lowest order in the Brueckner reaction matrix (BHF approximation), using the so-called *continuous choice* [15]. Motivated by the renewed interest in this subject, in the present paper we report an extension of the calculations of Ref. [12], along the following lines. First, in the calculations we make use of a different realistic nucleon-nucleon (NN) potential, i.e., the full Argonne V_{14} potential [16], which enables us to take into account a larger number of partial waves with respect to the calculation [12] with the separable Paris potential. These additional partial waves ($3\leqslant L\leqslant 6$) give a non-negligible contribution both to the EOS and the nucleon mean field, expecially in the high-density region, which is relevant for applications in astrophysics as well as in heavy-ion physics.

Second, the Bethe-Goldstone equation is now solved for the complex G matrix. This enables us to calculate the complex nuclear mean field and some closely related quantities such as the optical potential and the mean free path.

Third, according to the Landau definition of quasiparticle energy (for an extended discussion see Ref. [17]) in the calculations of the mass operator (nucleon self-energy) and single-particle properties, we go beyond the BHF approximation by including some higher-order correlation contributions. In particular, in the present work, we include the so-called *rearrangement* term M_2, which is a second-order diagram in the G matrix and accounts for particle-hole excitations in nuclear matter ground state. Next we consider also the *renormalization* contributions of the third and forth order in the G matrix, which account for the partial depletion of the neutron and proton Fermi seas due to the nuclear correlations [18]. It has been shown, in the case of pure neutron matter [19] and also symmetric nuclear matter [20], that the

*Permanent address: Institute of Modern Physics, Lanzhou, China.

new terms give a large contribution to s.p. properties like the mean field and the nucleon effective mass. We will refer to the present approach to compute nuclear s.p. properties as the extended Brueckner-Hartree-Fock (EBHF) approximation [19,20].

As is well known, the BHF approximation largely violates the Hugenholtz–Van Hove (HVH) theorem [21], which basically measures the consistency of a given order of approximation in a perturbative approach. In symmetric nuclear matter, the inclusion of the rearrangement contribution greatly improves the fulfillment of the HVH theorem [22]. In the present work, we study this problem in the case of asymmetric nuclear matter, within the EBHF approximation.

II. EBHF AND NUCLEON SELF-ENERGY FOR ASYMMETRIC NUCLEAR MATTER

In this section the formalism of the Brueckner-Bethe-Goldstone (BBG) theory is described for the case of asymmetry nuclear matter [12,23]. The proton and the neutron Fermi momenta are related to their corresponding densities ρ_p and ρ_n by the relations

$$k_F^p=\left[\frac{3\pi^2}{2}(1-\beta)\rho\right]^{1/3},$$

$$k_F^n=\left[\frac{3\pi^2}{2}(1+\beta)\rho\right]^{1/3},$$

where $\rho=\rho_p+\rho_n$ is the total density, and $\beta=(\rho_n-\rho_p)/\rho$ the asymmetry parameter determining the neutron excess (from now on we assume $\rho_n\geqslant\rho_p$).

The starting point in BBG theory is the Brueckner reaction matrix G, which in the case of asymmetric nuclear matter depends also on the isospin components of the two colliding nucleons. The G matrix satisfies the Bethe-Goldstone equation,

$$G(\rho,\beta;\omega)=v_{NN}+v_{NN}\sum_{k_1k_2}\frac{|k_1k_2\rangle Q(k_1,k_2)\langle k_1k_2|}{\omega-\epsilon(k_1)-\epsilon(k_2)+i\eta}G(\rho,\beta;\omega), \tag{1}$$

where v_{NN} is the two-body nuclear interaction, and ω is the starting energy. Here $k\equiv(\vec{k},\sigma,\tau)$ denotes s.p. momentum, spin, and isospin z components, respectively.

The G matrix can be considered as an in-medium effective interaction between two nucleons. The surrounding nucleons renormalize the bare NN interaction via the Pauli blocking and the nuclear mean field. The Pauli operator, defined as

$$Q(k_1,k_2)=[1-n(k_1)][1-n(k_2)], \tag{2}$$

prevents two nucleons in intermediate states from scattering into states inside their respective Fermi seas. By $n(k)$ we denote the Fermi distribution function, which at zero temperature is given by the step function $\theta(k-k_F^\tau)$ (uncorrelated ground state). The s.p. energy[1]

$$\epsilon(k)=\frac{\hbar^2k^2}{2m}+U(k) \tag{3}$$

appearing in the energy denominator of Eq. (1), involves the *auxiliary* potential $U(k)$, which controls the convergence rate of the hole-line expansion. Within the BHF approximation the neutron and proton s.p. auxiliary potentials are calculated from the real part of the on-shell antisymmetrized G matrix via the relation

$$U(k)=\sum_{k'}n(k')\mathrm{Re}\langle kk'|G[\epsilon(k)+\epsilon(k')]|kk'\rangle_A. \tag{4}$$

Here we adopt the continuous choice [15] for the auxiliary s.p. potential. In this context it has the physical meaning of the mean field that each nucleon feels during its propagation between two successive scatterings.

In the BHF approximation, Eqs. (1), (3), and (4) are solved self-consistently for a given total density ρ and asymmetry β. Then the energy per particle is evaluated at the lowest order (two hole-line diagrams) of the BBG hole-line expansion (see Ref. [23] for the case of asymmetric matter).

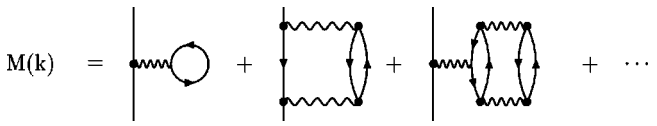

FIG. 1. Hole-line expansion of s.p. potential.

A. Mass operator and quasiparticle energy

One of the main purposes of the present paper is to calculate s.p. properties of neutrons and protons in asymmetric matter going beyond the BHF approximation. To this end we introduce the mass operator [15,24]

$$M^\tau(k,\omega)=V^\tau(k,\omega)+iW^\tau(k,\omega), \tag{5}$$

which is a complex quantity and can be identified with the potential energy felt by a neutron ($\tau=n$) or a proton ($\tau=p$) with momentum $\vec{k}$ and energy ω in asymmetric nuclear matter (hereafter we will write out explicitly the isospin index τ). In the same spirit of the BBG theory, the mass operator $M^\tau(k,\omega)$ can be expanded in a perturbation series according to the number of hole lines [25] and the various terms of this expansion can be represented by means of Goldstone diagrams a few of which are shown in Fig. 1.

In analogy with the case of symmetric nuclear matter, the neutron and proton quasiparticle energies $E^\tau(k)$ are the solutions of the energy-momentum relation

$$E^\tau(k)=\frac{\hbar^2k^2}{2m}+V^\tau[k,E^\tau(k)], \tag{6}$$

[1]In the present work, we assume the neutron and proton rest masses equal to their average value m.

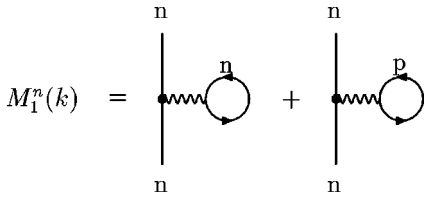

FIG. 2. The first-order hole-line expansion of neutron s.p. potential.

i.e., $E^\tau(k)$ is obtained from the on-shell values of the real part of the mass operator.

To the lowest order in the hole-line expansion the mass operator is given by (diagrams of Fig. 2)

$$M_1^\tau(k,\omega)=\sum_{\tau'}\sum_{k'\sigma'} n^{\tau'}(k')\langle kk'|G^{\tau\tau'}[\omega+\epsilon^{\tau'}(k')]|kk'\rangle_A \equiv\sum_{\tau'} M_1^{\tau\tau'}(k,\omega). \quad (7)$$

In this approximation the quasiparticle energy $E_1^\tau(k)$ coincides with the BHF s.p. energy given by Eqs. (3),(4), i.e., $E_1^\tau(k)=\epsilon^\tau(k)$.

B. The rearrangement contribution to the s.p. energy

The next contribution to the perturbative expansion of the mass operator is given by the so-called *rearrangement* term $M_2^\tau(k,\omega)$ [15]. The associated Goldstone diagrams are shown in Fig. 3. M_2^τ is a second-order diagram in the G matrix and accounts for particle-hole excitations in nuclear matter. Its expression, extended to asymmetric nuclear matter, reads

$$M_2^\tau(k,\omega)=\frac{1}{2}\sum_{\tau'}\sum_{k'\sigma'}[1-n^{\tau'}(k')]\sum_{k_1k_2} n^\tau(k_1)n^{\tau'}(k_2) \times\frac{|\langle kk'|G^{\tau\tau'}[\epsilon^\tau(k_1)+\epsilon^{\tau'}(k_2)]|k_1k_2\rangle_A|^2}{\omega+\epsilon^{\tau'}(k')-\epsilon^\tau(k_1)-\epsilon^{\tau'}(k_2)-i\eta} \equiv\sum_{\tau'} M_2^{\tau\tau'}(k,\omega), \quad (8)$$

where $\epsilon^\tau(k)$ is the s.p. spectrum in BHF approximation, given by Eqs. (3), (4). In this approximation for the mass operator [i.e., $M^\tau(k,\omega)\simeq M_1^\tau(k,\omega)+M_2^\tau(k,\omega)$] the quasiparticle energy (6) is given by the approximate relation

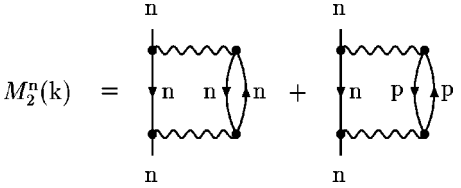

FIG. 3. The second-order hole-line expansion of neutron s.p. potential.

$$E_2^\tau(k)=E_1^\tau(k)+Z_2^\tau(k)V_2^\tau[k,E_1^\tau(k)] =\frac{\hbar^2k^2}{2m}+V_1^\tau[k,E_1^\tau(k)]+Z_2^\tau(k)V_2^\tau[k,E_1^\tau(k)], \quad (9)$$

where

$$Z_2^\tau(k)=\left\{1-\frac{\partial}{\partial\omega}[V_1^\tau(k,\omega)+V_2^\tau(k,\omega)]\right\}^{-1}_{\omega=E_1^\tau(k)} \quad (10)$$

is an approximation of the *quasiparticle strength* for asymmetric nuclear matter

$$Z^\tau(k)=\left\{1-\frac{\partial}{\partial\omega}[V^\tau(k,\omega)]\right\}^{-1}_{\omega=E^\tau(k)}. \quad (11)$$

C. The renormalization contributions to the s.p. energy

Due to many-body correlations the two Fermi seas are partially depleted, and the correlated momentum distributions $\tilde{n}^\tau(k)$ differ from the uncorrelated ones $n^\tau(k)=\theta(k-k_F^\tau)$. To account for this physical effect, one considers the contribution $M_3^\tau(k,\omega)$ (last diagram in Fig. 1) given by [15,18]

$$M_3^\tau(k,\omega)=-\sum_{\tau'}\sum_{h'\sigma'}\kappa_2^{\tau'}(h')\langle kh'|G^{\tau\tau'} \times[\omega+\epsilon^{\tau'}(h')]|kh'\rangle_A, \quad (12)$$

where h' refers to ''hole'' state with momentum smaller than k_F^τ, and

$$\kappa_2^{\tau'}(h')=-\left[\frac{\partial}{\partial\omega}M_1^{\tau'}(h',\omega)\right]_{\omega=\epsilon^{\tau'}(h')}$$

is at the lowest order the depletion of neutron (proton) Fermi sea [15,18], i.e., $\kappa_2^{\tau'}(h')$ is the probability that a neutron (proton) hole-state ($|\vec{h}'|\leqslant k_F^{\tau'}$) is empty. Let us consider now the sum

$$\tilde{M}_1^\tau(k,\omega)\equiv M_1^\tau(k,\omega)+M_3^\tau(k,\omega) =\sum_{\tau'}\sum_{h'\sigma'}[1-\kappa_2^{\tau'}(h')] \times\langle kh'|G^{\tau\tau'}[\omega+\epsilon^{\tau'}(h')]|kh'\rangle_A =\sum_{\tau'}\sum_{h'\sigma'}\tilde{n}_2^{\tau'}(h')\langle kh'|G^{\tau\tau'}[\omega+\epsilon^{\tau'}(h')]|kh'\rangle_A \quad (13)$$

$\tilde{n}_2^{\tau'}(h')=[1-\kappa_2^{\tau'}(h')]$ being the second-order approximation for the correlated momentum distribution. $\tilde{M}_1^\tau(k,\omega)$ is the so-called *renormalized* BHF approximation for the off-shell mass operator [compare to Eq. (7)].

An accurate approximation consists in using the average value of the depletion, which is

$$\kappa^{\tau'} = \kappa_2^{\tau'}(h' = 0.75 k_F^{\tau'}). \tag{14}$$

Then Eqs. (12), (13) yield

$$M_3^{\tau}(k,\omega) \approx -\sum_{\tau'} \kappa^{\tau'} M_1^{\tau\tau'}(k,\omega), \tag{15}$$

$$\tilde{M}_1^{\tau}(k,\omega) \approx \sum_{\tau'} [1-\kappa^{\tau'}] M_1^{\tau\tau'}(k,\omega). \tag{16}$$

From the similar considerations, a renormalization correction should also be brought from the four hole-line terms to the second-order contribution to M_2^{τ} in order to take into account the fact that the hole-state k_1 in Eq. (8) is partially empty (see also Ref. [18] for symmetric nuclear matter). Along the same lines of the previous correction one gets the *renormalized* M_2, which is approximately given by

$$\tilde{M}_2^{\tau}(k,\omega) = \sum_{\tau'} [1-\kappa^{\tau'}] M_2^{\tau\tau'}(k,\omega). \tag{17}$$

The renormalized contributions can also be traced to the functional dependence of the G matrix on the quasiparticle occupation numbers within the Landau theory of Fermi liquids. It can be shown, in fact, that taking the functional derivative of the binding energy (at two hole-line level) includes also the terms of third and fourth order in the self-energy, the effect of which has just been discussed. Taking into account all the corrections discussed above, from Eq. (6) one can get the following expression for the quasiparticle energy [18]:

$$E_3^{\tau}(k) = \frac{\hbar^2 k^2}{2m} + V_1^{\tau}[k, E_1^{\tau}(k)] + Z_3^{\tau}(k) \times \sum_{\tau'} \{-\kappa^{\tau'} V_1^{\tau\tau'}[k, E_1^{\tau}(k)] + (1-\kappa^{\tau'}) V_2^{\tau\tau'}[k, E_1^{\tau}(k)]\} \tag{18}$$

where

$$Z_3^{\tau}(k) = \left\{ 1 - \sum_{\tau'} (1-\kappa^{\tau'}) \frac{\partial}{\partial \omega} (V_1^{\tau\tau'}[k,\omega] + V_2^{\tau\tau'}[k,\omega]) \right\}^{-1}_{\omega = E_1^{\tau}(k)}. \tag{19}$$

In the following we refer to this approximation for the quasiparticle energy as the extended Brueckner-Hartree-Fock (EBHF) approximation [18–20].

D. Partial wave expansion and angular averaging

After the usual angular averaging on the Pauli operator and the energy denominator [26,22], the Bethe-Goldstone equation can be expanded in partial waves,

$$G_{\alpha LL'}^{\tau\tau'}(q,q',P,\omega) = v_{\alpha LL'}(q,q') + \frac{2}{\pi} \sum_{L''} \int q''^2 dq'' v_{\alpha LL''}(q,q'') \times \frac{\langle Q^{\tau\tau'}(q'',P)\rangle}{\omega - e_{12}^{\tau\tau'}(q'',P) + i\eta} \times G_{\alpha L''L'}^{\tau\tau'}(q'',q',P,\omega), \tag{20}$$

where $\vec{q} = (\vec{k}_1 - \vec{k}_2)/2$ and $\vec{P} = \vec{k}_1 + \vec{k}_2$ are the relative momentum and total momentum, respectively. $e_{12}^{\tau\tau'}(q'',P) = \langle \epsilon^{\tau}(k_1) + \epsilon^{\tau'}(k_2)\rangle$ is the angle average of the energy denominator. The angular-averaged Pauli operator is

(i) for $\tau = \tau'$ (neutron-neutron or proton-proton),

$$\langle Q^{\tau\tau}(q,P)\rangle = \begin{cases} \min(1,\xi_\tau) & \text{if} \quad \xi_\tau \geqslant 0 \\ 0 & \text{otherwise,} \end{cases} \tag{21a}$$

(ii) for $\tau \neq \tau'$ (neutron-proton or proton-neutron),

$$\langle Q^{\tau\tau'}(q,P)\rangle = \begin{cases} \dfrac{1}{2}[\min(1,\xi_p) + \min(1,\xi_n)] & \text{if} \quad \xi_n \geqslant -\xi_p, \xi_n \geqslant -1 \\ 0 & \text{otherwise,} \end{cases} \tag{21b}$$

where

$$\xi_\tau = \frac{P^2/4 + q^2 - (k_F^{\tau})^2}{Pq}.$$

The mass operators M_1 and M_2 become

$$M_1^{\tau\tau'}(k,\omega) = \frac{1+\delta_{\tau,\tau'}}{2\pi} \sum_{\alpha L} (2J+1) \int_0^{k_F^{\tau'}} k'^2 dk' \sin\theta d\theta G_{\alpha LL}^{\tau\tau'}[q,q,P,\omega + \epsilon^{\tau'}(k')], \tag{22a}$$

$$M_2^{\tau\tau'}(k,\omega)=\frac{2(1+\delta_{\tau,\tau'})}{\pi^2 k}\sum_{\alpha LL'}(2J+1)\int\int qdqPdP[1-n^{\tau'}(\sqrt{P^2/2+2q^2-k^2})]$$

$$\times\int q'^2dq'\langle R^{\tau\tau'}(q',P)\rangle\frac{|G^{\tau\tau'}_{\alpha LL'}[q,q',P,e_{12}^{\tau\tau'}(q',P)]|^2}{\omega+\epsilon^{\tau'}(\sqrt{P^2/2+2q^2-k^2})-e_{12}^{\tau\tau'}(q',P)-i\eta}. \tag{22b}$$

The integrations of q and P in the expression of M_2 are limited to

$$q_{\min}=\begin{cases}\max\left[0,\quad k-\frac{1}{2}(k_F^\tau+k_F^{\tau'}),\quad \frac{1}{2}(k_F^{\tau'}-k)\right] & \text{if}\quad k\leqslant k_F^\tau\\ \max\left[\frac{1}{2}\sqrt{2k^2-2(k_F^\tau)^2+(k_F^\tau-k_F^{\tau'})^2},\quad \frac{1}{2}(k+k_F^{\tau'})\right] & \text{if}\quad k>k_F^\tau\end{cases} \tag{23a}$$

$$q_{\max}=k+\frac{1}{2}(k_F^\tau+k_F^{\tau'}), \tag{23b}$$

and

$$P_{\min}=\begin{cases}\max[2(k-q),\ \sqrt{2k^2+2(k_F^{\tau'})^2-4q^2}] & \text{if}\quad q\leqslant\frac{1}{2}(k+k_F^{\tau'})\\ 2|q-k| & \text{if}\quad k>\frac{1}{2}(k+k_F^{\tau'})\end{cases} \tag{24a}$$

$$P_{\max}=\min[2(k+q),\ (k_F^\tau+k_F^{\tau'})]. \tag{24b}$$

The angular averaging of the anti-Pauli operator $R^{\tau\tau'}(k_1,k_2)\equiv n^\tau(k_1)n^{\tau'}(k_2)$ can be written as

(i) for $\tau=\tau'$, i.e., neutron-neutron or proton-proton

$$\langle R^{\tau\tau}(q,P)\rangle=\begin{cases}\min(1,\eta_\tau) & \text{if}\quad \eta_\tau\geqslant 0\\ 0 & \text{otherwise,}\end{cases} \tag{25a}$$

(ii) for $\tau\neq\tau'$, i.e., neutron-proton or proton-neutron

$$\langle R^{\tau\tau'}(q,P)\rangle=\begin{cases}\frac{1}{2}[\min(1,\eta_p)+\min(1,\eta_n)] & \text{if}\quad \eta_p\geqslant-\eta_n,\ \eta_p\geqslant-1\\ 0 & \text{otherwise,}\end{cases} \tag{25b}$$

where $\eta^\tau=-\xi^\tau$.

III. RESULTS

We have performed a set of nuclear matter calculations for the asymmetric case within the EBHF approximation. Three different densities have been selected: $\rho_0/2$, ρ_0, and $2\rho_0$, being $\rho_0=0.17\ \text{fm}^{-3}$ the saturation density of symmetric nuclear matter. For each density the whole range of asymmetry parameter ($0\leqslant\beta\leqslant 1$) has been spanned. The self-consistent solution of the Bethe-Goldstone equation yielding simultaneously G matrix and auxiliary potential $U^\tau(k)$ needed five iterations to reach a satisfactory convergence. The bare potential adopted as input in the calculation was the Argonne V_{14} [16] with 24 channels up to $L=6$.

A. Symmetry energy

In Fig. 4 (left panel) we report the results (symbols) for the energy per nucleon $B(\rho,\beta)$, as calculated self-consistently within the BHF approximation [23]. $B(\rho,\beta)$ is plotted as a function of β^2, for three values of density. The numerical results lie on a linear fit performed with only the first three values of the asymmetry parameter. This proves that the empirical parabolic law

$$B(\rho,\beta)=B(\rho,0)+E_{\text{sym}}(\rho)\beta^2, \tag{26}$$

taken from the nuclear mass table can be extended up to the highest asymmetry of nuclear matter, in good agreement with our previous BHF calculation with separable Paris potential [12].

Equation (25) can be considered as the β^2 expansion of the binding energy truncated at the lowest order. Only even powers of the asymmetry parameter β may occur in the expansion for charge-independent NN interactions, such as the Argonne V_{14} used in the present work. A β^4 contribution might arise at the three hole-line order of the BBG expansion. Unfortunately, no such calculation for $B(\rho,\beta)$ has been

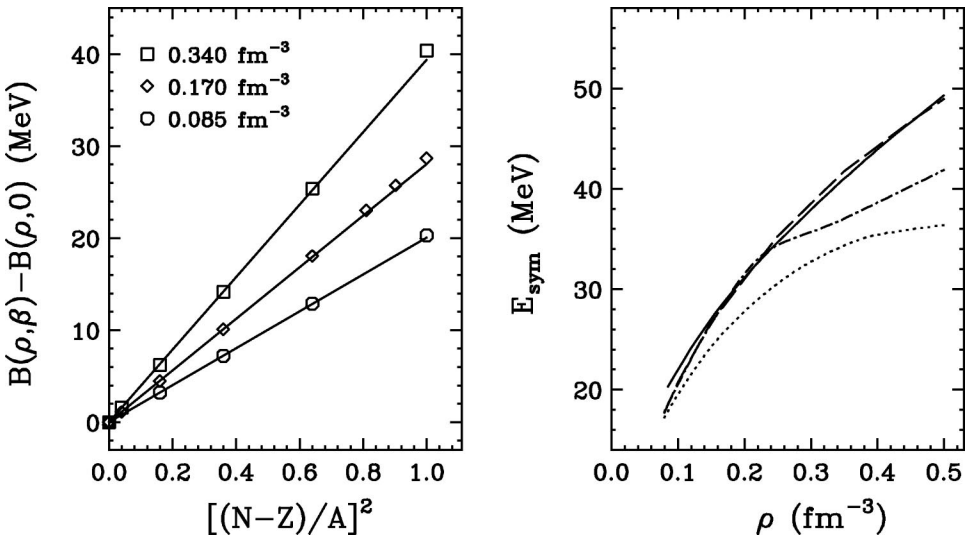

FIG. 4. Left panel: Total binding energy per nucleon in the range $0 \leqslant \beta^2 \leqslant 1$ at three densities as compared with the parabolic fits (straight lines) obtained from the first three values of β (0.0, 0.2, 0.4). Right panel: Density dependence of the symmetry energy of the present work (solid curve) using Argonne V_{14} as bare interaction in comparison with other nonrelativistic calculations. The dashed curve is the result of the lowest-order constrained variational calculation using Argonne V_{14} as bare interaction from Ref. [5]. The dotted and dot-dashed curves are the results of the variational approach using Argonne V_{14} and Argonne V_{14}+UVII, respectively, taken from Ref. [3].

done yet. However, it has been shown recently that the three hole-line contribution to the binding energy of symmetric nuclear matter [27] is rather small within the continuous choice. Therefore, we do not expect a large deviation from the parabolic law after including the three hole-line contribution. A deviation from the parabolic law could be expected at densities higher with respect to those considered in the present paper [5,7–9].

The symmetry energy is defined as

$$E_{\rm sym}(\rho) = \frac{1}{2}\left[\frac{\partial^2 B(\rho,\beta)}{\partial \beta^2}\right]_{\beta=0}. \tag{27}$$

Due to the simple β^2 law the symmetry energy can be equivalently calculated as the difference between the binding energy of pure neutron matter and symmetric nuclear matter: $E_{\rm sym}(\rho) = B(\rho,1) - B(\rho,0)$, but one would refrain from using that recipe at very high density. The results of our BHF calculations for $E_{\rm sym}(\rho)$ are depicted by the continuous curve in the right panel of Fig. 4. In the same figure, we show the results from the variational approach using the same Argonne V_{14} potential [3].

The systematic disagreement displayed by the two many-body approaches has been believed to be a shortcoming of the Brueckner approach in view of the fact that the BHF result lies above the ''variational'' one. However, in Ref. [3] (and similar works), the variational expectation value $E_{\rm var}$ of the Hamiltonian is calculated in a diagrammatic cluster expansion (FHNC-SOC), which is of course truncated to some order. To estimate the convergence of this diagrammatic cluster expansion, we plot, in the same figure, the results of a lowest-order constrained variational calculation [5], which includes only two-body cluster contributions to $E_{\rm var}$. Moreover, the variational trial wave function used in Ref. [3] does not contain the correlations which arise from L^2, $L^2(\sigma_i \cdot \sigma_j)$, and $(L \cdot S)^2$ terms of the nucleon-nucleon potential. Finally, spin-orbit correlations are not treated accurately, as discussed in the same paper [3]. All these NN correlations are included in a self-consistent way in the BHF approach. All the above-mentioned approximations could give large uncertainties in the calculated expectation value of the energy in the high density region. The same discrepancy has also been observed in our previous calculations for asymmetric nuclear matter [12] and also in neutron matter calculations [28].

From the previous discussion we guess that the nice agreement between our calculation and a lowest order constrained variational calculation [5] is fortuitous. On the other hand, the agreement up to $\rho \sim 0.24$ fm^{-3} with the variational calculation including three-body force [3], also plotted in Fig. 4, is hardly understandable.

More recent versions of the NN potential do not provide any appreciable difference of the symmetry energy from the present calculation except the CD-Bonn potential as discussed in Ref. [29]. All Brueckner calculations predict the symmetry energy to increase with the nucleon density and no saturation is observed up to $\rho = 0.5$ fm^{-3} at variance with the preceeding variational results [3]. In the relativistic mean-field theory this behavior is easily understood in terms of the ρ-meson exchange, which leads to a repulsive symmetry potential at all densities [1,9]. In order to try to explain what happens in the nonrelativistic case, we report in Fig. 5 the different contributions to the symmetry energy, plotted as a function of density. The kinetic contribution monotonically increases as $\rho^{2/3}$ according to the free Fermi-gas model. In the figure (right two panels), the isoscalar and isovector contributions of the potential part are plotted separately. As already found in the previous paper [12], the most important contribution to the $T=0$ component is due to the deuteron $^3S_1$-$^3D_1$ coupled channels of the interaction, which exhibits

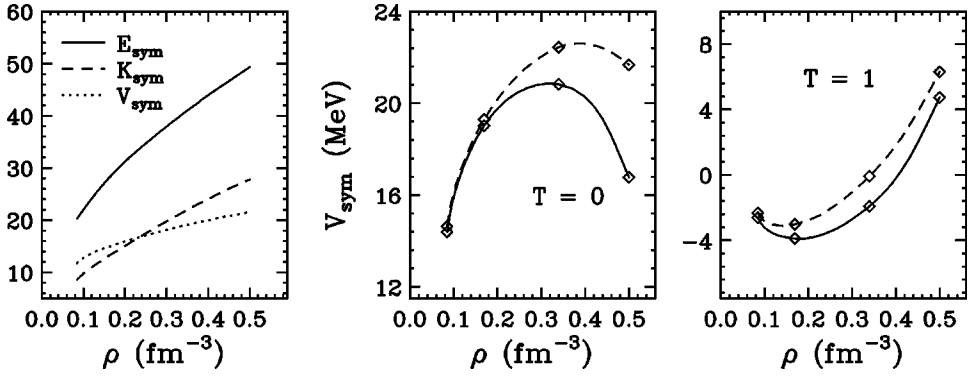

FIG. 5. Symmetry energy vs density in BHF approximation. Left panel: total symmetry energy ($E_{\rm sym}$), kinetic ($K_{\rm sym}$), and potential ($V_{\rm sym}$) contributions (only Argonne V_{14}). Middle panel: potential contribution from isospin $T=0$ channels with Argonne V_{14} (solid curve) and separable Paris (dashed curve) potentials. Right panel: potential contribution from isospin $T=1$ channels with Argonne V_{14} (solid curve) and separable Paris (dashed curve) potentials.

a maximum at $\rho\simeq 0.3$ fm^{-3}. This peak can be traced back to the behavior of the two components: the attractive $^3S_1$ channel dominates at low energy whereas the repulsive $^3D_1$ dominates at high energy. Two terms compensate each other at the energy $E\simeq 4E_F\simeq 200$ MeV, where E_F is the Fermi energy corresponding to $\rho\simeq 0.3$ fm^{-3}.

B. Single-particle energy

For asymmetric nuclear matter the neutron mass operator M^n is different from the proton mass operator M^p. Moreover, as shown in Figs. 2 and 3 [see also Eqs. (7),(8)], both of them can be split into two components: $M^p=M^{pp}+M^{pn}$ for protons and $M^n=M^{nn}+M^{np}$ for neutrons. In Fig. 6 the on-shell values of the real part of M_1^τ are reported as a function of the s.p. momentum, for different values of the asymmetry parameter β at fixed density $\rho=0.17$ fm^{-3}. The proton mean field $V_1^p(k)\equiv \mathrm{Re}\,M_1^p(k)$ becomes more attactive, while the neutron mean field $V_1^n(k)\equiv \mathrm{Re}\,M_1^n(k)$ becomes more repulsive going from symmetric ($\beta=0$) to neutron ($\beta=1$) matter. The β dependence of V_1^n and V_1^p is almost linear and nearly symmetric with respect to their common value at $\beta=0$. This result supports from a microscopic point of view the validity of the so-called Lane potential [30]. It is worth noticing (see Fig. 6, upper panels) that a crossing point occurs for both V_1^p and V_1^n, where the isospin effect on neutron and proton mean field versus β is inverted. This behavior of the neutron and proton mean fields can be understood in terms of phase-space arguments, as already pointed out in Ref. [12]. To this end, we write the single-particle potentials, V_1^n and V_1^p, in terms of their components $V_1^{\tau\tau'}$ [defined according to Eq. (7)]:

$$V_1^p(k)\simeq \frac{1}{2}(1-\beta)\rho\langle G^{pp}\rangle+\frac{1}{2}(1+\beta)\rho\langle G^{pn}\rangle, \qquad (28)$$

$$V_1^n(k)\simeq \frac{1}{2}(1-\beta)\rho\langle G^{np}\rangle+\frac{1}{2}(1+\beta)\rho\langle G^{nn}\rangle, \qquad (29)$$

where $\langle G^{pp}\rangle$ is the average value of the real part of the matrix G^{pp} in the proton Fermi sphere ($|\vec{h}'|\leqslant k_F^p$), $\langle G^{pn}\rangle$ is the average value of the real part of the matrix G^{pn} in the neutron Fermi sphere ($|\vec{h}'|\leqslant k_F^n$), and $\langle G^{nn}\rangle$, $\langle G^{np}\rangle$ have similar definitions. This approximation is suggested by the almost linear dependence of V_1^n and V_1^p on β and, in fact, is numerically fulfilled with a good accuracy (see also Fig. 8). The crossing point in momentum space is determined by the occurrence of $\langle G^{pp}\rangle=\langle G^{pn}\rangle$ for V_1^p and $\langle G^{np}\rangle=\langle G^{nn}\rangle$ for V_1^n at a certain value of the momentum which does not depend upon β. A signature of the inversion of the isospin effect at the crossing point could be found in those collective observables measured in heavy-ion collisions which are sensitive to the momentum dependence of the mean field.

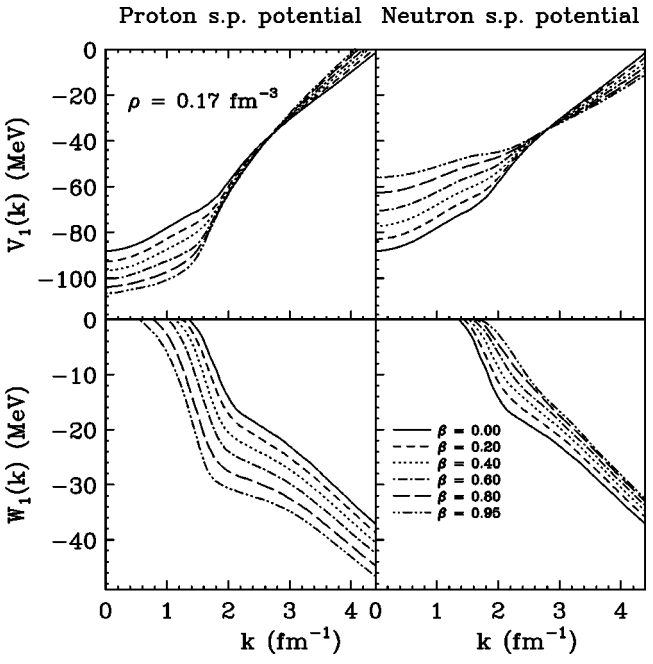

FIG. 6. Real part (upper panels) and imaginary part (lower panels) of the first-order single-particle potentials M_1 for proton (left panel) and neutron (right panel), respectively, as a function of momentum for different asymmetry parameters at density $\rho=0.17$ fm^{-3}.

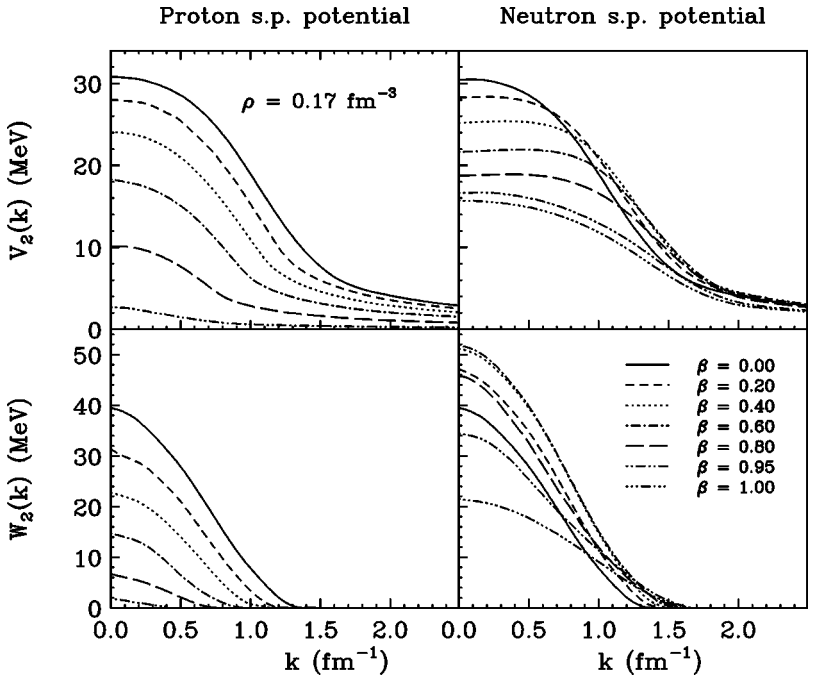

FIG. 7. Real part (upper panels) and imaginary part (lower panels) of the second-order single-particle potentials M_2 for proton (left panel) and neutron (right panel), respectively, as a function of momentum for different asymmetry parameters at density $\rho=0.17$ fm^{-3}.

The imaginary part W_1^τ of the mass operator M_1^τ is due to the virtual collisions of a single nucleon with a neutron or a proton of the background, promoting it to a particle state. W_1^τ is vanishing below the Fermi momentum k_F^τ due to the Pauli blocking. It is worth noticing that reducing the proton Fermi momentum implies less Pauli blocking for protons. This means that high asymmetric nuclear matter is less transparent to the proton propagation.

The second-order terms of the on-shell mass operator M_2^τ are plotted in Fig. 7. The real part V_2^τ (upper panels) gives the contribution to the mean field due to the coupling of the single-particle motion with the ground-state particle-hole excitations. As is well known, V_2^τ is repulsive and reduces to a large extent the pure BHF mean field V_1^τ which is too attractive compared with the phenomenological optical potential [26].

The imaginary part W_2^τ plays a role complementary to W_1^τ: it describes the virtual collisions of a single nucleon of the background with an excited neutron or proton, making it to decay into a hole state. W_2^τ is vanishing above the Fermi momentum k_F^τ.

In order to focus on only the isospin dependence, we plot in Fig. 8 the mass operator as a function of the β at $k=0$ fm^{-1} except for the imaginary part of M_1 for which a value of k above the Fermi momentum has to be taken.

The first-order contribution has the linear behavior for the real part as well as for the imaginary part as expected from phase-space arguments. The slope of $|W_1^{pn}|$ is more pronounced than that of $|W_1^{np}|$ since the neutron particle-hole excitations coupled to a proton in a particle state are more favored than the proton particle-hole excitations coupled to a neutron (see also Fig. 6).

The isospin dependence of the second-order contribution M_2^τ is affected by the coupling between the nucleon hole states and particle-hole excitations [see the bubble in Fig. 3 and Eq. (8)], which yields a nonlinear variation of the mixed components M_2^{pn} and M_2^{np} vs β. The nonlinearity is much more sizable for V_2^{pn} and W_2^{np}, which can be easily explained as a phase-space effect as well, i.e., of the interplay between the neutron and proton phase spaces as increasing neutron excess.

C. Fermi energy and Hugenholtz–Van Hove theorem

The EBHF approximation basically relies on the Landau definition of quasiparticle energy as shown in Sec. I, whose relation to the Brueckner theory is well established [31]. Study of the Hugenholtz–Van Hove (HVH) theorem [21] within the EBHF approximation could provide an additional support to a proper definition of the quasiparticle energy and, at the same time, a more realistic evaluation of the Fermi energy. Strictly speaking, the HVH theorem concerns only symmetric nuclear matter at saturation point ($P=0$), and it states that the energy per nucleon must be exactly equal to the Fermi energy. In the case of asymmetric nuclear matter (two-component system) at zero temperature, the HVH theorem can be generalized via the thermodynamic relation

$$\frac{E(\rho,\beta)}{A}+\frac{P(\rho,\beta)}{\rho}=Y^pE_F^p(\rho,\beta)+Y^nE_F^n(\rho,\beta), \quad (30)$$

$P(\rho,\beta)$ being the pressure and $Y^p=\rho_p/\rho$ and $Y^n=\rho_n/\rho$ the proton and neutron fractions, respectively. The Fermi energy is calculated from the quasiparticle energy spectrum at Fermi surface according to Eq. (6). In Table I it is numerically

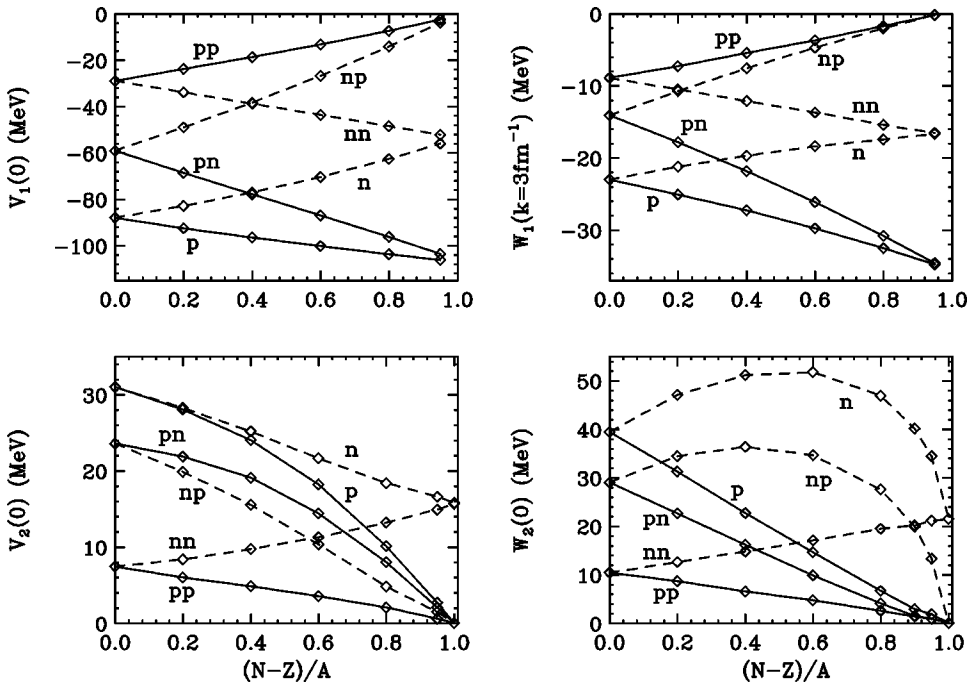

FIG. 8. Different components of the first-order (upper panels) and the second-order (lower panels) single-particle potentials at density $\rho=0.17$ fm^{-3} for suitable values of momentum vs asymmetry parameters. For the real part of M_1 and M_2, and the imaginary part of M_2, the momentum is $k=0$, while for the real part of M_1 the momentum is $k=3$ fm^{-1}.

shown to what extent the HVH theorem is fulfilled by the EBHF approximation. The pressure has been calculated using the relation $P(\rho,\beta)=\rho^2[\partial E(\rho,\beta)/\partial\rho]$. In the fourth column the left-hand side of Eq. (30) is calculated for several asymmetries (density fixed at $\rho=0.17$ fm^{-3}). One would notice that, despite the fact that the total density is fixed at the empirical saturation value, our calculated saturation point lies at higher density, because, as is well known, Brueckner theory with two-body force misses the empirical saturation density. The last three columns provide different approximations for the right-hand side of Eq. (30). The pure BHF approximation by itself is far from fulfilling the HVH theorem. Including the unrenormalized ground-state correlations (indicated by BHF$+M_2$ in the table), where the Fermi energy is calculated according to Eq. (9), provides some improvement but it is not enough to fulfill the HVH theorem. One needs to include both the rearrangement and the renormalized contributions (EBHF) if a satisfactory agreement within less than 10% is to be attained (last column of Table I). This result is in keeping with the uncertainty in the calculation of the pressure because the binding energy curve is rather flat as a function of density.

IV. APPLICATIONS

A. Effective mass

The effective mass incorporates the nonlocal part of the mean field which makes the local part less attractive for a nucleon traveling with momentum $k>0$. It is defined as

$$\frac{m_\tau^*(k)}{m}=\frac{k}{m}\left(\frac{dE^\tau(k)}{dk}\right)^{-1}. \tag{31}$$

TABLE I. As a function of the asymmetry parameter (first column) the physical quantities involved in the Hugenholtz–Van Hove theorem are reported (in MeV): pressure over ρ (second column), energy per nucleon (third column), and ''weighted'' chemical potentials of asymmetric nuclear matter in different approximations, as discussed in the text. $Y^p=Z/A$ and $Y^n=N/A$ are the proton and neutron fractions, respectively. The total density is $\rho=0.17$ fm^{-3}.

β	P/ρ	E/A	$P/\rho+E/A$	$Y^pE_F^p+Y^nE_F^n$ BHF	$Y^pE_F^p+Y^nE_F^n$ BHF$+M_2$	$Y^pE_F^p+Y^nE_F^n$ EBHF
0.0	−5.02	−15.92	−20.94	−34.27	−28.50	−19.28
0.2	−4.40	−14.73	−19.13	−32.29	−26.43	−17.35
0.4	−3.27	−11.36	−14.63	−26.28	−20.74	−12.42
0.6	0.08	−5.75	−5.67	−16.56	−11.44	−4.41
0.8	3.76	2.24	6.00	−2.40	2.07	7.42
1.0	8.91	12.83	21.74	16.28	19.67	22.39

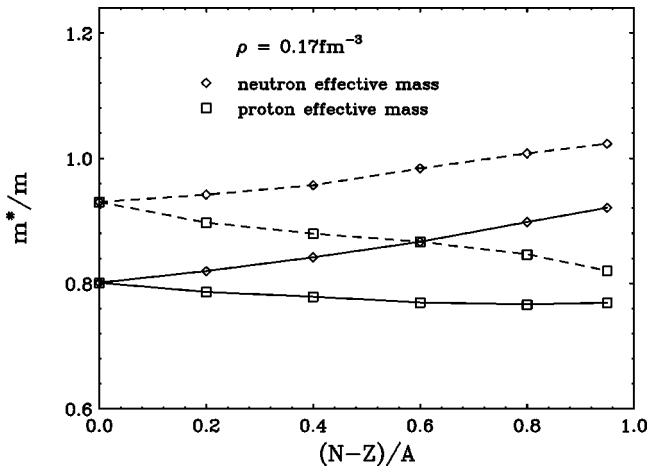

FIG. 9. Proton and neutron effective masses vs asymmetry parameter at density $\rho=0.17$ fm^{-3}. The solid curves are results from the pure BHF calculation, while the dashed curves are calculated from the EBHF (including the renormalization contributions).

The momentum dependence of m^* is characterized by the wide bump inside the Fermi sphere due to the high probability amplitude for particle-hole excitations near the Fermi surface [15]. The effect of correlations is a flattening of the slope of the mean field around the Fermi energy, which implies an enhancement of the effective mass at k_F with respect to BHF value [19,20]. This result is shown in Fig. 9, where an increase from 0.8 to 0.92 is observed for symmetric nuclear matter at the saturation density. Also shown in the figure is the isospin dependence of the neutron (upper curve) and proton (lower curve) effective masses. In both the BHF and EBHF calculations, m_n^* increases and m_p^* decreases as increasing β. Compared to the BHF approximation, the corrections of EBHF shift m_n^* and m_p^* to higher values, a feature which can be traced to the depletions of the proton and neutron Fermi surfaces due to the ground-state correlations. The value of m_p^* calculated from EBHF approaches its BHF value as increasing β since the correlations become smaller.

B. Mean free path

Information on the in-medium cross section or, equivalently, on the mean free path of a nucleon traveling inside a nuclear medium can be obtained from the transparency of a nucleus measured in $(e,e'p)$ reactions [32] and, in general, from nucleon-induced reactions at low energy [33]. The underlying assumption is that the behavior of a nucleon located at the position $\vec{r}$ in a nucleus is the same as a nucleon in nuclear matter at density $\rho(\vec{r})$. Such an assumption is the well-known local density approximation (LDA) [34]. The mean free path is intimately related to the imaginary part of the optical potential or, equivalently, to the imaginary part of the mean field. The latter comes from the collisions of a single nucleon with the background of neutrons and protons: a nucleon with momentum $k \geqslant k_F$ can collide with a neutron or proton of its Fermi sea and promote it to a particle state, or a nucleon with momentum $k \leqslant k_F$ interacting with an excited neutron or proton can make it decay into a hole state. The first process is related to the imaginary part of M_1, the second one to the imaginary part of M_2, both of which have been plotted in the lower panels of Figs. 6 and 7. But, in the case of asymmetric matter the collisions between like and unlike nucleons yield contributions to the mean field which are very different.

The mean free path λ_τ is given by

$$\lambda_\tau(E)=\frac{\hbar^2 k(E)}{2\tilde{m}_\tau}\frac{1}{|\mathrm{Im}\,M_\tau[k(E),E]|},$$

where $\tilde{m}_\tau$ is the so-called k mass, and E is the single-particle energy [35]. In Fig. 10 the proton (upper panels) and neutron (lower panels) mean free paths calculated within the EBHF approximation are shown for three values of the total density. In each panel the values of λ_τ for several asymmetries are plotted as a function of single-particle energy. The most relevant effect of the isospin asymmetry is the increasing deviation from the symmetric values (solid lines), upward for λ_n and downward λ_p, as increasing asymmetry. The nonvanishing values of neutron and proton mean free paths below their respective Fermi energies are effects of ground-state correlations, which prevents a full occupancy of the Fermi spheres. Comparing with the BHF calculation it turns out that the correlation effects tend to rise the asymptotic value of the mean free path from about 3 fm up to about 4 fm at the saturation density of symmetric nuclear matter [20].

In Fig. 11 it is shown how the isospin dependence of the inverse λ develops as increasing nuclear matter densities at a fixed value of the energy. Except for very small asymmetries the shift of λ_p and λ_n is not symmetric with respect to their common value at $\beta=0$. At any density the slope of the neutron inverse λ is less than the proton one. This effect can be traced to the reduction, as increasing neutron excess, of the proton particle-hole excitations contributing to the neutron optical potential (see Figs. 6 and 7). Moreover, the EBHF λ_n seems to reach the asymptotic value of pure neutron matter much faster than in the uncorrelated case.

The most striking effect of the isospin-asymmetry is the sizable reduction of the proton mean free path at high asymmetry. Accordingly, the nuclear surface would become more transparent to neutrons than protons in nucleon-induced reactions on nuclei near the neutron drip-line. This effect would be more pronounced at higher density as shown in Fig. 11.

C. Proton fraction in β-equilibrium matter

The core of a neutron star is expected to be formed by an uncharged mixture of neutrons, protons, electrons, and muons in equilibrium with respect to the weak interactions (β-stable matter). The concentrations of different particles are then obtained under the requirements

$$\mu_n-\mu_p=\mu_e, \quad \mu_\mu=\mu_e, \tag{32}$$

$$\rho_p=\rho_e+\rho_\mu. \tag{33}$$

The difference between the neutron and proton chemical potentials can be expressed as

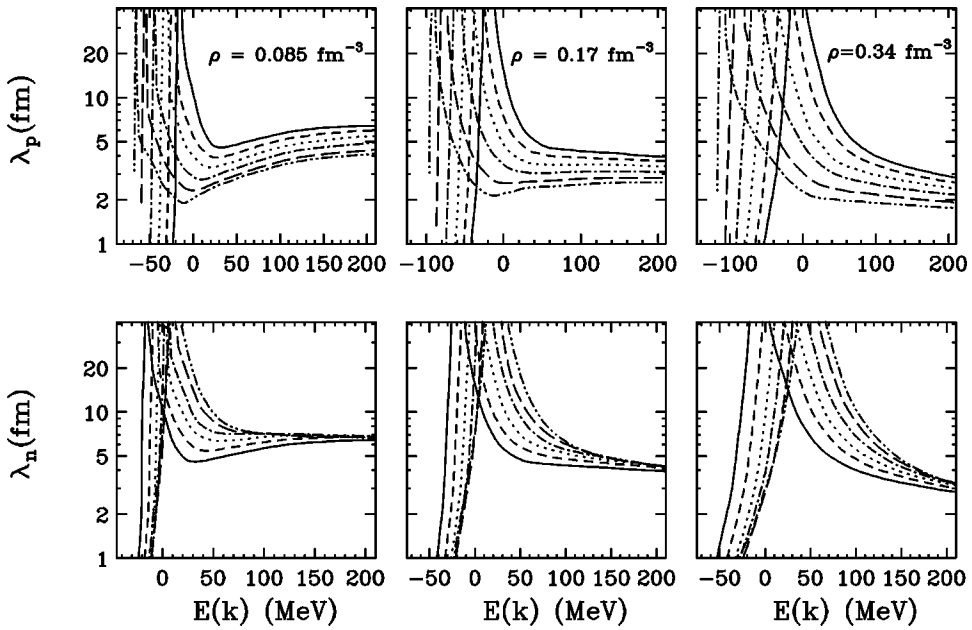

FIG. 10. The energy dependence of proton (upper panels) and neutron (lower panels) mean free paths for different asymmetry parameters at three densities $\rho=0.085$ fm^{-3}, $\rho=0.17$ fm^{-3}, and $\rho=0.34$ fm^{-3}. Only EBHF results are reported. The different kinds of lines correspond to different asymmetry parameters with the same notation as in Fig. 6.

$$\mu_n-\mu_p=-\left.\frac{\partial B}{\partial Y^p}\right|_\rho=2\left.\frac{\partial B}{\partial \beta}\right|_\rho . \tag{34}$$

In the parabolic approximation, Eq. (25), for the energy per particle of asymmetric nuclear matter, one has

$$\mu_n-\mu_p=4E_{\rm sym}(\rho)(1-2Y^p). \tag{35}$$

Therefore, the composition of β-stable matter, and in particular, the proton fraction Y^p present at a given density, is strongly dependent on the nuclear symmetry energy. The proton fraction plays also a crucial role in the thermal evolution of neutron stars. In fact, if the proton fraction in the core of a neutron star is above a critical value $Y^p_{\rm Urca}$, the so-called direct Urca processes can occur [36–38]. If they occur, the direct Urca processes enhance the neutrino emission and neutron star cooling rate by a large factor compared to the standard cooling scenario. The critical proton fraction has been estimated [36] to be in the range 11–15 %. In a recent paper [28], based on microscopic EOS of dense matter, it has been found that the onset of direct Urca processes occurs at densities $\rho>0.54$–0.65 fm^{-3}, depending on the nuclear interaction used to get the EOS (see Ref. [28] for more details).

In Table II, we report our present calculations for the proton fraction $Y^p(\rho)$ for β-stable matter in comparison with the one obtained with the separable Paris (see Ref. [12]) and variational calculation of Ref. [16] with the Argonne V_{14} potential plus the Urbana model (UVII) three-body force. In the calculations reported in Table II, muons have not been included.

Our purpose, in the present paper, is not an accurate determination of the proton fraction in dense stellar matter. Here, we aim to study how the inclusion of contributions beyond the BHF to the chemical potentials could alter the proton fraction in β-stable matter. In fact, to solve the β-equilibrium conditions (32),(33), the shift between neutron and proton chemical potentials $\hat{\mu}\equiv\mu_n-\mu_p$ has to be evaluated. In Table III the neutron and proton chemical potentials

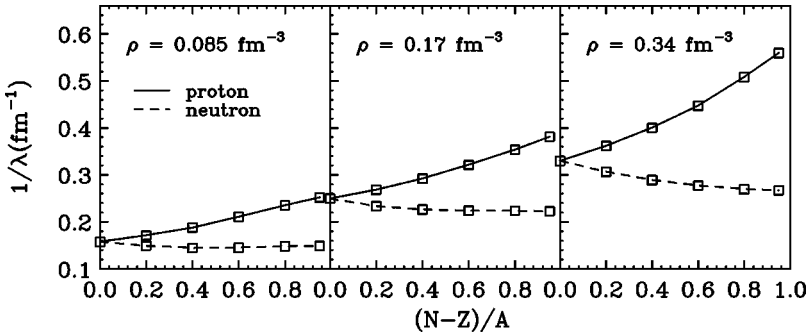

FIG. 11. Proton and neutron inverse mean free paths vs asymmetry parameter for three densities $\rho=0.085$ fm^{-3}, $\rho=0.17$ fm^{-3}, and $\rho=0.34$ fm^{-3} at a fixed single-particle energy $E^\tau(k)=180$ MeV from the EBHF calculation.

TABLE II. Proton fraction in β-stable nuclear matter (no muons) vs the total baryonic density from different forces. The values reported are $10^2 Y$. The results in the second column are taken from BL. Those in the third column have been given by A. Fabrocini (private communication).

ρ_B	Paris	AV14+UVII	Present
0.038	2.75	—	
0.076	2.80	1.85	2.40
0.11	3.09	2.48	2.74
0.14	3.48	2.96	3.03
0.17	3.70	3.37	3.32
0.20	4.10	3.74	3.50
0.30	4.90	3.67	4.07
0.40	5.79	3.56	4.57
0.50	—	3.63	5.01

and their difference $\hat{\mu}$, are reported for the different approximations used in the present work. From the results reported in Table III we see that the chemical potential, approximated by the Fermi energy, in the EBHF is noticeably affected by the rearrangement and renormalization contributions. However, their difference and consequently the proton fraction is almost unchanged with respect to the BHF approximation. The EBHF approximation provides neutron and proton Fermi energies, which are in better agreement with the empirical values extracted from the mass table of atomic nuclei [39] than the BHF approximation [12].

V. CONCLUSIONS

In this paper we have reported the study of asymmetric nuclear matter within the Brueckner-Bethe-Goldstone approach. The isospin effect on the equation of state has been investigated by performing a set of calculations at the two hole-line level of the BBG expansion for the energy per particle $B(\rho,\beta)$. The Bethe-Goldstone equation has been solved with the Argonne V_{14} interaction. The continuous choice has been adopted for the auxiliary potential since it makes the convergence of the hole-line expansion faster than the gap choice [27]. Ranging the asymmetry parameter from $\beta=0$ (symmetric nuclear matter) to $\beta=1$ (pure neutron matter) it was possible to check that $B(\rho,\beta)$ exhibits a linear dependence on β^2 for baryonic densities as large as at least two times the saturation density. This result confirms the empirical law introduced in the mass formula of atomic nuclei and also extends its validity up to the highest asymmetries. As a consequence, the entire isospin effect is incorporated in the symmetry energy. The calculation of the symmetry energy in the BHF approximation shows a monotonic increase as a function of baryonic density. Its value calculated at the saturation density is about 28.7 MeV, in agreement with the empirical one. The comparison with the variational prediction is made rather difficult due to the contradictory results still existing in this approach. An accurate determination of the symmetry energy is required for dynamical simulations of collisions between neutron-rich nuclei, where the collective observables including collective flows, balance energy, and other quantities are expected to be sensitive to the isospin degree of freedom [1,2]. Ground-state correlations were included in the mass operator up to the four hole-line order contributions. Their effect on the single particle properties has been investigated. The first-order contribution to the mass operator displays a linear dependence on the asymmetry parameter confirming a long-standing analysis by Lane [30]. A new effect of the isospin degree of freedom appears when the ground-state correlations induced by the second-order contribution are introduced in the mass operator. That is a nonlinear effect due to the particle-hole excitations of, say, protons induced by the propagation of a neutron in the nuclear medium. This feature affects the isospin dependence of single-particle properties such as mean field, effective mass, and the mean free path. Along with the symmetry energy the heavy-ion collisions with asymmetric nuclei could also probe the isospin dependence of mean free path

TABLE III. Proton and neutron chemical potentials (Fermi energies) calculated in different approximations and compared with the symmetry energy. The results corresponding to four values of the asymmetry parameter β for each of the three densities are reported.

ρ	β	μ^p	μ^n	$\hat{\mu}$	μ^p	μ^n	$\hat{\mu}$	μ^p	μ^n	$\hat{\mu}$	$4\beta E_{\rm sym}$
($\rm fm^{-3}$)			BHF			BHF+M_2			EBHF		
	0.2	−33.99	−18.05	15.94	−30.44	−14.18	16.26	−23.00	−6.92	16.08	16.22
0.085	0.4	−42.98	−10.77	32.20	−39.75	−7.01	32.74	−32.60	−0.16	32.44	32.45
	0.6	−51.71	−3.31	48.40	−49.26	0.15	49.41	−43.24	5.67	48.91	48.67
	0.8	−61.32	3.68	65.00	−59.63	6.58	66.21	−54.85	10.49	65.34	64.90
	0.2	−45.94	−23.19	22.75	−40.45	−17.08	23.37	−31.01	−8.24	22.77	23.00
0.170	0.4	−58.08	−12.65	45.43	−53.46	−6.72	46.74	−44.30	1.25	45.55	46.00
	0.6	−71.73	−2.77	68.96	−68.10	2.72	70.82	−59.60	9.39	68.99	69.00
	0.8	−86.22	6.91	93.13	−83.99	11.63	95.62	−76.42	16.73	93.15	92.00
	0.2	−47.53	−16.11	31.42	−38.89	−5.75	33.14	−24.04	7.12	31.16	32.30
0.340	0.4	−64.84	−1.79	63.05	−57.48	8.88	66.36	−42.31	20.22	62.53	64.59
	0.6	−82.75	12.21	94.96	−77.17	22.85	900.02	−62.44	32.35	94.79	96.89
	0.8	−103.15	25.48	128.63	−99.87	35.52	135.39	−86.32	42.95	129.27	129.18

and effective mass, which play also an important role in the collisional dynamics.

The EBHF approximation for asymmetric matter results in a satisfactory fulfillment of the Hugenholtz–Van Hove theorem in all asymmetry range $0 \leqslant \beta \leqslant 1$. This property makes us more confident of the hole-line expansion of the mass operator for calculating the single-particle properties including the Fermi energy. We found that the neutron and proton chemical potentials are largely affected by contributions beyond the BHF approximation. This could have far reaching consequences for the physics of the neutron star crust. In fact, the proton chemical potential in asymmetric nuclear matter is a very important ingredient in locating the inner boundary of the neutron star crust. However, the difference $\hat{\mu} = \mu^n - \mu^p$, and consequently the proton fraction in β-stable matter, is almost unchanged in the EBHF approximation with respect to the BHF approximation.

ACKNOWLEDGMENT

The authors are indebted to Professor A. Fabrocini for valuable discussions.

[1] B. A. Li, C. M. Ko, and W. Bauer, Int. J. Mod. Phys. E **7**, 147 (1998).
[2] M. Di Toro, V. Baran, M. Colonna, G. Fabbri, A. B. Larionov, S. Maccarone, and S. Scalone, Prog. Part. Nucl. Phys. **42**, 125 (1999).
[3] R. B. Wiringa, V. Fiks, and A. Fabrocini, Phys. Rev. C **38**, 1010 (1988).
[4] A. Akmal and V. R. Pandharipande, Phys. Rev. C **56**, 2261 (1997).
[5] G. H. Bordbar and M. Modarres, Phys. Rev. C **57**, 714 (1998).
[6] B. ter Haar and R. Malfliet, Phys. Rev. Lett. **59**, 1652 (1987); R. Malfliet, Nucl. Phys. **A488**, 721c (1988).
[7] L. Engvik, M. Hjorth-Jensen, E. Osnes, G. Bao, and E. Ostgaard, Phys. Rev. Lett. **73**, 2650 (1994); Astrophys. J. **469**, 794 (1996).
[8] H. Huber, F. Weber, and M. K. Wiegel, Phys. Rev. C **51**, 1790 (1995); **57**, 3488 (1998).
[9] C. H. Lee, T. T. S. Kuo, G. Q. Li, and G. E. Brown, Phys. Rev. C **57**, 3488 (1998).
[10] N. Frölich, H. Baier, and W. Bentz, Phys. Rev. C **57**, 3447 (1998).
[11] F. de Jong and H. Lenske, Phys. Rev. C **57**, 3099 (1998).
[12] I. Bombaci and U. Lombardo, Phys. Rev. C **44**, 1892 (1991).
[13] J. Haidenbauer and W. Plessas, Phys. Rev. C **30**, 1822 (1984); **32**, 1424 (1985).
[14] M. Lacombe, B. Loiseaux, J. M. Richard, R. Vinh Mau, J. Côté, D. Pirés, and R. de Tourreil, Phys. Rev. C **21**, 861 (1980).
[15] J. P. Jeukenne, A. Lejeune, and C. Mahaux, Phys. Rep., Phys. Lett. **25C**, 83 (1976).
[16] R. B. Wiringa, R. A. Smith, and T. L. Ainsworth, Phys. Rev. C **29**, 1207 (1984).
[17] G. E. Brown, Rev. Mod. Phys. **43**, 1 (1971).
[18] M. Baldo, I. Bombaci, G. Giansiracusa, U. Lombardo, C. Mahaux, and R. Sartor, Phys. Rev. C **41**, 1748 (1990).
[19] W. Zuo, G. Giansiracusa, U. Lombardo, N. Sandulescu, and H. J. Schulze, Phys. Lett. B **421**, 1 (1998).
[20] W. Zuo, U. Lombardo, and H. J. Schulze, Phys. Lett. B **432**, 241 (1998).
[21] N. M. Hugenholtz and L. Van Hove, Physica (Amsterdam) **24**, 363 (1958).
[22] M. Baldo, I. Bombaci, L. S. Ferreira, G. Giansiracusa, and U. Lombardo, Phys. Rev. C **43**, 2605 (1991).
[23] I. Bombaci, T. T. S. Kuo, and U. Lombardo, Phys. Rep. **242**, 165 (1994).
[24] C. Mahaux and R. Sartor, Adv. Nucl. Phys. **20**, 1 (1991).
[25] J. Hüfner and C. Mahaux, Ann. Phys. (N.Y.) **73**, 525 (1972).
[26] P. Grangé, J. Cugnon, and A. Lejeune, Nucl. Phys. **A473**, 365 (1987).
[27] H. Q. Song, M. Baldo, G. Giansiracusa, and U. Lombardo, Phys. Rev. Lett. **81**, 1584 (1998).
[28] M. Baldo, I. Bombaci, and G. F. Burgio, Astron. Astrophys. **328**, 274 (1997).
[29] L. Engvik, M. Hjorth-Jensen, R. Machleidt, H. Müther, and A. Polls, Nucl. Phys. **A627**, 85 (1997).
[30] A. M. Lane, Nucl. Phys. **35**, 676 (1962).
[31] S.-O. Bäckmann, G. E. Brown, and J. A. Niskanen, Phys. Rep. **124**, 1 (1985).
[32] V. R. Pandharipande and S. C. Pieper, Phys. Rev. C **45**, 791 (1992).
[33] M. Avrigeanu, A. Harangozo, V. Avrigeanu, and A. N. Antonov, Phys. Rev. C **54**, 2538 (1996); **56**, 1633 (1997).
[34] P. Ring and P. Schuck, *The Nuclear Many-Body Problem* (Springer-Verlag, New York, 1980).
[35] C. Mahaux, Phys. Rev. C **28**, 1848 (1983).
[36] J. M. Lattimer, C. J. Pethick, M. Prakash, and P. Haensel, Phys. Rev. Lett. **66**, 2701 (1991).
[37] M. Baldo, J. Cugnon, A. Lejeune, and U. Lombardo, Nucl. Phys. **A536**, 349 (1992).
[38] K. A. Van Riper, B. Link, and R. I. Epstein, Astrophys. J. **448**, 294 (1995).
[39] J. P. Jeukenne, C. Mahaux, and R. Sartor, Phys. Rev. C **43**, 2211 (1991).